Breaking the open-circuit voltage deficit floor in PbS quantum dot solar cells through synergistic ligand and architecture engineering

Santanu Pradhan[1], Alexandros Stavrinadis[1], Shuchi Gupta[1], Sotirios Christodoulou[1] and Gerasimos Konstantatos[1, 2]*

[1] ICFO-Institut de Ciencies Fotoniques, The Barcelona Institute of Science and Technology, 08860 Castelldefels (Barcelona), Spain

[2] ICREA—Institució Catalana de Recerca i Estudis Avançats, Passeig Lluís Companys 23, 08010 Barcelona, Spain

* gerasimos.konstantatos@icfo.es

ABSTRACT: To realize the full potential of colloidal quantum dot (CQD) based solar cells, it is important to address the issue of large open circuit voltage (V_{OC}) deficit which is a major roadblock in reaching higher efficiencies. The origin of the V_{OC} deficit in these solar cells lies primarily in the presence of sub-bandgap trap states of the QDs. Here, we present a synergistic engineering framework to passivate these sub-bandgap states in PbS QDs through chemical surface passivation and remote passivation exploiting ligand and architecture engineering. In particular we form bulk nano-heterojunctions (BNH) by mixing PbS QDs with ZnO nanocrystals in conjunction with mixed ligand treatments to passivate surface traps. We employ the mixed ligand system of zinc iodide and 3-mercatopropyonic acid (MPA) to leverage the benefits of both organic and inorganic ligands for surface passivation and improved charge transport. This mixed ligand treatment in BNH architectures leads to record low Voc deficit for PbS QDs of 0.4 V - 0.55 V compared to previously reported 0.6 -0.8 V for the range of 1.1 – 1.35 eV bandgap PbS QDs.

Solution processed colloidal quantum dot (CQD) solar cells, mainly comprising lead sulphide (PbS), are one of the most promising class of low-cost, high-efficiency third generation solar cells thanks to their solution processability, bandgap tuning with quantum confinement and stability[1-4]. Recent developments in the field have reached over 11% power conversion efficiency (PCE) [5]. Despite these improvements, colloidal quantum dot based solar cells fall behind when it comes to the achievable Voc, which is a significant factor in exploiting the bandgap tunability offered by this class of photovoltaic materials. Although the best performing devices show considerably large short circuit current (I_{SC}) and fill factor (FF), their V_{OC} of around 0.6 V for nearly 1.3 eV bandgap QDs remains lower than half the bandgap[5, 6]. The difference of V_{OC} from the respective material bandgap (E_g), known as V_{OC} deficit ($\frac{E_g}{q} - V_{OC}$), is thus considerably large in case of colloidal quantum dot based solar cells. Further improvement of solar cell efficiency depends on addressing the challenge to reduce this large V_{OC} deficit without a major compromise of other parameters. Although the origin of this large Voc deficit in this class of solar cells has not been consolidated fully, the presence of subband-gap states, introduced due to unpassivated surface, residual surfactants, off-stoichiometry, and surface oxidation are considered the main determinant factor [7-9].

Several approaches have been adapted to reduce the V_{OC} deficit namely, reducing interface recombination loss[10,11], reducing bulk recombination through remote trap passivation[12], passivating the surface with core-shell structure[13] and maintaining charge neutrality of the QDs[14]. It has been shown that interface recombination does not play a major role in V_{OC} deficit in PbS QD based solar cells whereas the bulk recombination in the active layer is believed to influence the V_{OC} loss due to the presence of emissive sub bandgap traps [15]. Supressing sub-bandgap traps with electron rich nanocrystals was successfully demonstrated by Rath et. al[16], employing bulk nano heterojunctions (BNH) of PbS and ZnO nanocrystals with 3- mercaptopropionic acid (MPA) as the ligand exchange treatment. While

this approach showed remarkable reduction in V_{OC} deficit, the short circuit current density (Jsc) of the devices was limited due to poor charge transport and high series resistance. On the other hand, recent high efficiency PbS QD based PV devices are passivated with organic halides (TBAI, EMII etc) that have improved charge collection yet the Voc remains low [6,17]. This prompted us to use mixed ligands comprising both organic and inorganic components in bulk nanoheterojunction architectures. We have previously reported that a mixed ligand treatment comprised of zinc iodide (ZnI_2) and MPA can reduce the emissive traps and improve efficiency for PbS QD based solar cell [18]. Further in this work we demonstrate that this hybrid ligand passivation facilitates the formation of ZnO/PbS based BNH architectures and at the same time improves charge collection efficiency leading to record Voc values for CQD solar cells.

Figure 1(a) shows the focused ion beam (FIB) cross-sectional micrograph of the BNH device. The BNH was prepared by mixing colloidal ZnO and PbS nanocrystals in an optimized 1:3 weight ratio (optimization of the mixing ratio for the device performance is shown in supporting Figure S1). The active layer consisted of 12 layers of BNH over a ZnO base layer (experimental details in supporting information S1). The final top two layers of PbS were treated with 1, 2 Ethanedithiol (EDT) to act as the electron blocking layer[6] as shown in Figure 1(b). The photovoltaic performance of the BNH devices are shown in Figure 1(c). The best performing device showed a V_{OC} of 0.69 V with an average J_{SC} of 20.4 mA/cm^2. The cell exhibited a PCE of 7.6% significantly higher than previously reported MPA treated BNH devices (PCE 5.2%) with reported J_{SC} of 16.30 mA/cm^2 and V_{OC} of 0.64 V [16]. The forward and reverse I-V scans confirmed the low hysteresis in these devices. These devices also showed improved performance in sub sun illumination (10% sun) similar to the previously reported MPA treated BNH[16]. Under 10% sun illumination, the device showed an improved PCE of 9.1% with J_{SC} 2.44 mA/cm^2, V_{OC} 0.63 V and FF of 0.59 (supporting information S3). The devices were kept in air and it was observed that the PCE was within 15% of the maximum

value even after 55 days (supporting information S4). The external quantum efficiency (EQE) spectra of the device is shown in Figure 1(d) consistent with the AM1.5 measured J_{SC} (19.6 mA/cm^2 as calculated from EQE spectra). Fabry-Perot cavity effect is visible in the EQE spectra due to thick BNH layer formation. A first direct indication of the improved V_{OC} lies on the lower reverse saturation dark current[19] and the high rectification ratio as shown in the inset of Figure 1(c). To further corroborate the suppressed trap-assisted recombination achieved in our devices, congruent with the formation of the BNH, we measured the Voc dependence on the light intensity which yields an ideality factor (**η**) approaching unity (supporting information S5), suggestive of band to band carrier recombination[16].

The high V_{OC} of the BNH devices tempted us to study the V_{OC} dependence of this class of devices with various sizes (and thus bandgap) of PbS QDs of the devices. We have achieved V_{OC} as high as 0.8V for 1.34 eV bandgap PbS quantum dots (supporting information S6). To our knowledge, this is the highest reported V_{OC} for any PbS quantum dot based solar cell. We have plotted the V_{OC} of the BNH and bilayer devices (both utilizing the same mixed ligand approach) as a function of QD bandgap (E_g) (Figure 2(a)). The BNH V_{OC} can be fitted as, $\left\{V_{OC} = \frac{E_g}{q}(0.712) - 0.164\right\}V$ compared to the bilayer devices V_{OC} relation $\left\{V_{OC} = \frac{E_g}{q}(0.574) - 0.0406\right\}V$. This is a remarkable feature considering the Schockley-Queisser limit[20] for V_{OC} as $\sim (\frac{E_g}{q} - 0.2)\ V$. It is noteworthy that the previously reported high-V_{OC} CQD PbS solar cells followed the relation $V_{OC} = \left\{\frac{E_g}{q}(0.553) - 0.059\right\}V$ in which the slope is considerably lower than the one reported herein[21].

To gain further insight of the physical processes in the devices and the role of the BNH architecture, we have performed a series of opto-electronic characterizations. Transient photo voltage (TPV) and photo current (TPC) of devices were measured with applying different

optical bias to get the recombination dynamics and trap states. By comparing the BNH devices with the bilayer devices we can verify the hypothesis of remote trap passivation with BNH formation: Figure 2(b) shows the comparison of recombination lifetime and the recombination rate for the BNH and bilayer devices. Higher recombination lifetime and lower recombination rate indicate lower recombination loss in the case of BNH devices which is consistent with the increased V_{OC}. Further, we have projected the in-gap trap states density combining the TPV and TPC data in figure 2(c). This clearly shows the lowering of in-gap density of states in the case of BNH devices compared to bilayer ones. The lowering of trap state density is a clear evidence of remote trap passivation with the mixture of electron rich ZnO nanocrystals in PbS QD matrix. This is also supported by the lowering of Urbach tail energy (E_U) as extracted from the EQE spectra (supporting information S7). E_U decreases from 23.5 meV for bilayer device to 19.6 meV for BNH device. The low temperature analysis of V_{OC} gives the indication of presence of emissive sub-band gap due to traps in the devices. Figure 2(d) shows temperature dependent V_{OC} plot for bilayer and BNH devices. Extrapolation of temperature dependent V_{OC} plot at 0 K yields 1.16 V for the BNH device with PbS QDs of 1.21 eV bandgap (bandgap measured from EQE onset and verified with photoluminescence (PL) data), whereas the bilayer device shows an extrapolation close to 1 V for similar bandgap PbS QDs. These findings are consistent with previous reports and further support our claim of remote trap passivation with BNH formation[15, 16].

PL data can further enlighten the role of BNH in remote trap passivation for PbS quantum dot based solar cells. Figure 3(a) shows the normalised PL spectra for bilayer and BNH devices treated with ZnI_2 and MPA mixture. For both BNH and bilayer the band-edge emission peak was observed around 1.20 eV with hardly a difference of 10 meV. The latter may have originated due to the difference in dielectric media in BNH and bilayer QD solids and confirms that there is no change in the PbS QD bandgap. On the other hand, a significant

difference was observed in the longer wavelength region: Sub-band gap emission was observed for bilayer devices throughout the region of 0.77-1.10 eV range with the centre around 0.91 eV, whereas only band edge emission was detected from BNH devices. To gain further insight on the nature of the emissive species we plot the PL intensity (I) with the incident power (p) and have fitted with the equation $I \propto p^n$, where n is the power exponent (Figure 3(b)). For bilayer, the band-edge emission follows a super linear dependence (n∼1.42) consistent with previous reports[15, 22] whereas for BNH device, the response follows a nearly linear (n∼0.98) correlation with incident power. The linear correlation observed in the BNH structures corresponds to direct recombination whereas the super-linear dependence, present in the bilayer case, is due to the progressive saturation of sub-bandgap traps. To further corroborate this, we have measured the dependence of the band-edge and sub-bandgap emission on light intensity. By increasing the incident excitation intensity the ratio of the band-edge emission to the sub-bandgap emission decreases (supporting information S8) for the bilayer case, consistent with the model of sub bandgap trap state saturation.

In Figure 4 we plot the V_{OC} deficit of the BNH devices and compare with several other standard solar cell devices as well as prior reports on PbS CQD solar cells. C-Si[23], GaAs[24] and recently developed perovskite based solar cells[25] show lower V_{OC} deficit (0.3 V to 0.4 V) and hence better V_{OC} with high efficiency whereas CZTSSe[26], CdTe[27], QD based solar cells display much higher V_{OC} deficit (0.6V to 0.8 V) which is a major obstacle for these solar cells to reach the full potential. We have also compared V_{OC} deficit with several PbS QD based solar cells. The basic ZnO/PbS depleted heterojunction solar cells[15] show a V_{OC} deficit of 0.58 V to 0.78 V. The V_{OC} deficit improved with TiO_2/PbS depleted heterojunction[28], hybrid passivation[5], Schottky junction[21] and core-shell formation[13]. We have found that, mixed ligand treatments can reduce the V_{OC} deficit in bilayer devices[18] which varies as $(0.426)\frac{E_g}{q}$. In this work we

demonstrate that further significant improvement in Voc is achieved by the utilization of this mixed ligand treatment in BNH architectures with the Voc deficit varying as $(0.288)\frac{E_g}{q}$.

In summary, we have presented a methodology to reduce the V_{OC} deficit PbS QD based solar cells. The mixed ligand treatment on the BNH reduces the V_{OC} deficit as well as increases the current density compared to previously reported MPA treated BNH devices. Improved V_{OC}, FF and J_{SC} ultimately increases the device efficiency by 46% (5.2% to 7.6%). It should be noted that the bilayer devices that employ the mixed ligand treatment have thus far achieved higher PCE (of 9.9%) compared to the BNH reported herein, yet their Voc is lowered by 50 -60 mV compared to the BNH devices. This is due to the yet to be optimized charge transport along the ZnO percolation path in the BNH devices and our work points to the use of appropriate ligand treatments that have the potential to improve this further. The use of the ZnI_2 in combination with MPA has resulted in a significant improvement in that aspect over the prior reports of MPA treated BNH devices and further progress can be expected by further optimization along this front. We have also presented a series of different characterizations to prove the role of BNH in trap passivation and hence lowering V_{OC} deficit in case of PbS QD based solar cells. Although, this is a significant step towards producing high efficiency PbS solar cells with high V_{OC}, the incorporation of ZnO inside the PbS QD matrix affects the optical absorption as well as the charge transport. Addressing these challenges can pave the way for high efficiency PbS QDs with even lower V_{OC} deficit.

Acknowledgments

We acknowledge financial support from the European Research Council (ERC) under the European Union's Horizon 2020 research and innovation programme (grant agreement No 725165), the Spanish Ministry of Economy and Competitiveness (MINECO) and the "Fondo Europeo de Desarrollo Regional" (FEDER) through grant MAT2014-56210-R. This work was also supported by

AGAUR under the SGR grant (2014SGR1548) and by European Union H2020 Programme under grant agreement n°696656 Graphene Flagship. We also acknowledge financial support from Fundacio Privada Cellex, the CERCA Programme and the Spanish Ministry of Economy and Competitiveness, through the "Severo Ochoa" Programme for Centres of Excellence in R&D (SEV-2015-0522).

References:

(1) Nozik, A. J.; Beard, M. C.; Luther, J. M.; Law, M.; Ellingson, R. J.; Johnson, J. C. *Chem. Rev.* **2010**, 110, 6873–6890.

(2) Carey, G. H.; Abdelhady, A. L.; Ning, Z.; Thon, S. M.; Bakr, O. M.; Sargent, E. H. *Chem. Rev.* **2015**, 115, 12732–12763.

(3) Yuan, M.; Liu, M.; Sargent, E. H. *Nat. Energy* **2016**, 1, 16016

(4) Loiudice, A.; Rizzo, A.; Grancini, G.; Biasiucci, M.; Belviso, M. R.; Corricelli, M.; Curri, M. L.; Striccoli, M.; Agostiano, A.; Cozzoli, P. D.; Petrozza, A.; Lanzanidh, G.; Gigliabc, G. *Energy Environ. Sci.* **2013**, 6, 1565-1572.

(5) Liu, M.; Voznyy, O.; Sabatini, R.; Garcia de Arquer, F. P.; Munir, R.; Balawi, A. H.; Lan, X.; Fan, F.; Walters, G.; Kirmani, A. R.; Hoogland, S.; Laquai, F.; Amassian, A; Sargent, E. H. *Nat. Mater.* **2017**, 16, 258-263.

(6) Chuang, C.-H. M.; Brown, P. R.; Bulović, V.; Bawendi, M. G. *Nat. Mater.* **2014**, 13, 796– 801.

(7) Ip, A. H.; Thon, S. M.; Hoogland, S.; Voznyy, O.; Zhitomirsky, D.; Debnath, R.; Levina, L.; Rollny, L. R.; Carey, G. H.; Fischer, A.; Kemp, K. W.; Kramer, I. J.; Ning, Z.; Labelle, A. J.; Chou, K. W.; Amassian, A.; Sargent, E. H. *Nat. Nanotechnol.* **2012**, 7, 577– 582.

(8) Bae, W. K.; Joo, J.; Padilha, L. A.; Won, J.; Lee, D. C.; Lin, Q.; Koh, W.; Luo, H.; Klimov, V. I.; Pietryga, J. M. *J. Am. Chem. Soc.* **2012**, 134, 20160– 20168.

(9) Weidman, M. C.; Beck, M. E.; Hoffman, R. S.; Prins, F.; Tisdale, W. A. *ACS Nano* **2014**, 8, 6363–6371.

(10) Yuan, M.; Voznyy, O.; Zhitomirsky, D.; Kanjanaboos, P.; Sargent, E. H.; *Adv. Mater.* **2015**, 27, 917-921.

(11) Jin, Z.; Yuan, M.; Li, H.; Yang, H.; Zhou, Q.; Liu, H.; Lan, X.; Liu, M.; Wang, J.; Sargent, E. H.; Li, Y. *Adv. Funct. Mater.* **2016**, 26, 5284–5289.

(12) Rath, A. K.; Bernechea, M.; Martinez, L.; Garcia de Arquer, F. P.; Osmond, J.; Konstantatos, G. *Nat. Photon.* **2012**, 6, 529–534.

(13) Neo, D. C. J.; Cheng, C.; Stranks, S. D.; Fairclough, S. M.; Kim, J. S.; Kirkland, A. I.; Smith, J. M.; Snaith, H. J.; Assender, H. E; Watt, A. A. R. *Chem. Mater.*, **2014**, *26*, 4004–4013.

(14) Ko, D.-K.; Maurano, A.; Suh, S. K.; Kim, D.; Hwang, G. W.; Grossman, J. C.; Bulović, V.; Bawendi, M. G. *ACS Nano*, **2016**, 10, 3382–3388.

(15) Chuang, C.-H. M.; Maurano, A.; Brandt, R. E.; Hwang, G. W.; Jean, J.; Buonassisi, T; Bulović, V.; Bawendi, M. G. *Nano Lett.*, **2015**, 15, 3286–3294.

(16) Rath, A. K.; Garcia de Arquer, F. P.; Stavrinadis, A.; Lasanta, T.; Bernechea, M.; Diedenhofen, S. L.; Konstantatos, G. *Adv. Mater.* **2014**, 26, 4741– 4747.

(17) Cao, Y.; Stavrinadis, A.; Lasanta, T.; So, D.; Konstantatos, G. *Nat. Energy*, **2016**, 1, 16035.

(18) Pradhan, S.; Stavrinadis, A.; Gupta, S.; Bi, Y.; Di Stasio, F.; Konstantatos, G. *Small*, **2017** (DOI: 10.1002/smll.201700598).

(19) Potscavage, Jr., W. J.; Yoo, S.; Kippelen, B.; *Appl. Phys. Lett.*, **2008**, 93, 193308 (1-3).

(20) Shockley, W.; Queisser, H. J. *J. Appl. Phys.* **1961**, 32, 510– 519.

(21) Yoon, W.; Boercker, J. E.; Lumb, M. P.; Placencia, D.; Foos, E. E.; Tischler, J. G. *Sci. Rep.* **2013**, 3,2225.

(22) Schmidt, T.; Lischka, K.; Zulehner, W. *Phys. Rev. B* **1992**, 45, 8989– 8994.

(23) Masuko, K.; Shigematsu, M.; Hashiguchi, T.; Fujishima, D.; Kai, M.;Yoshimura, N.; Yamaguchi, T.; Ichihashi, Y.; Mishima, T.; Matsubara, N.; Yamanishi, T.; Takahama, T.; Taguchi, M.; Maruyama, E.; Okamoto, S. *IEEE J. Photovolt.* **2014**, 4, 1433-1435.

(24) Kayes, B. M.; Nie, H.; Twist, R.; Spruytte, S. G.; Reinhardt, F.; Kizilyalli, I. C.; Higashi, G. S. PVSC, **2011**, 4-8 (DOI: 10.1109/PVSC.2011.6185831).

(25) Yang, W. S.; Noh, J. H.; Jeon, N. J.; Kim, Y. C.; Ryu, S.; Seo, J.; Seok, S. II. *Science*, **2015**, 348, 1234-1237.

(26) Wang, W.; Winkler, M. T.; Gunawan, O.; Gokmen, T.; Todorov, T. K.; Zhu, Y.; Mitzi, D. B. *Adv. Energy Mater*. **2013**, 4, 1301465.

(27) Gloeckler, M.; Sankin, I.; Zhao, Z. *IEEE J. Photovolt.* **2013**, 3, 1389 – 1393.

(28) Speirs, M. J.; Dirin, D. N.; Abdu-Aguye, M.; Balazs, D. M.; Kovalenko, M. V.; Loi, M. A. *Energy Environ. Sci.,* **2016**, 9, 2916-2924.

Figures:

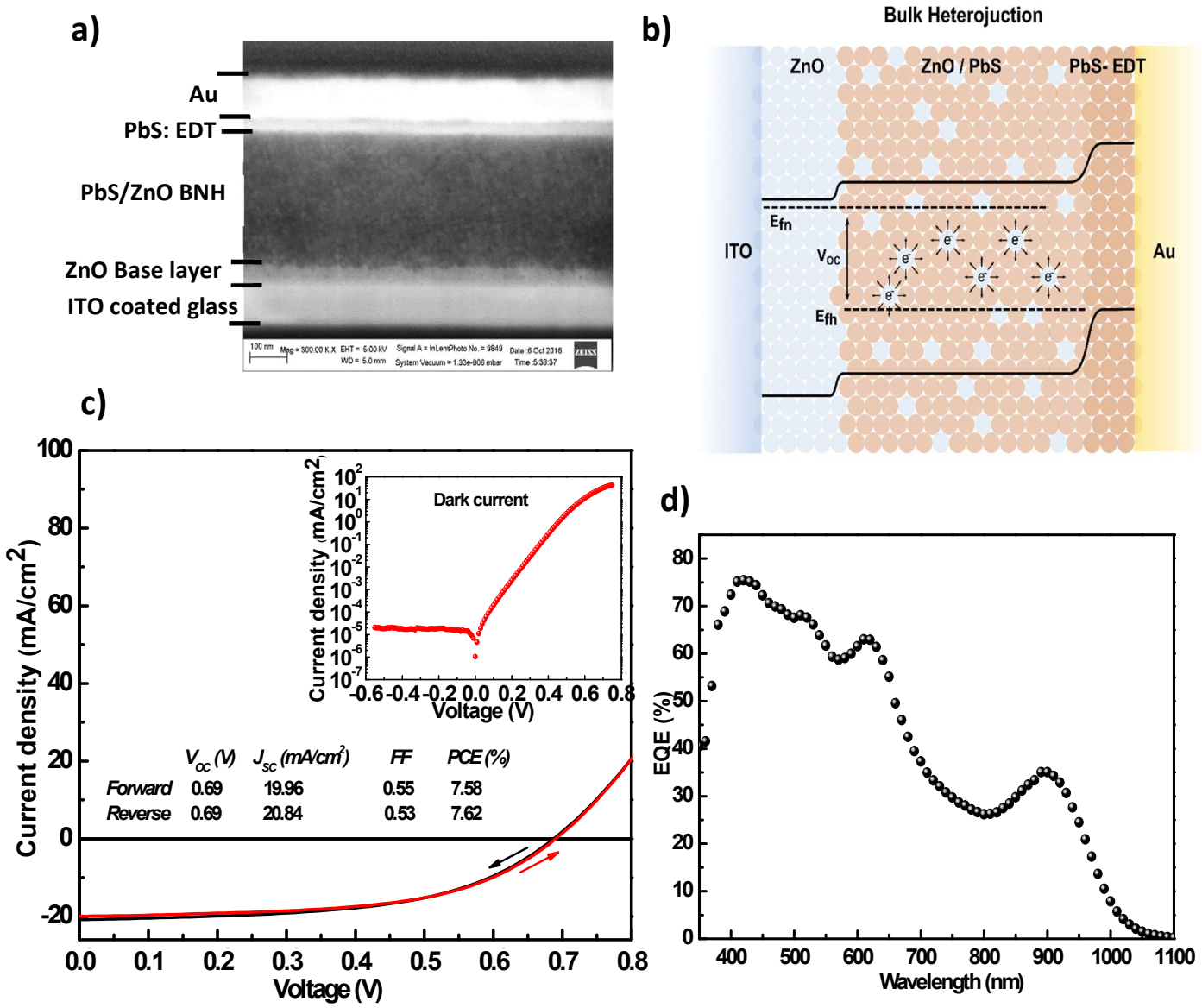

Figure 1: (a) FIB cross-sectional micrograph of the BNH device. (b) Schematic diagram of the BNH device with corresponding energy level positions. The BNH layer was prepared by mixing ZnO and PbS QDs. The remote traps in PbS QDs are passivated by the electrons from ZnO and hence increase the electron quasi Fermi level in BNH layer and ultimately improve the V_{OC} of the devices. (c) J-V plot of BNH devices with forward and backward sweep to calculate the PV performance. Inset parameters are the figures of merit of the champion device. (Inset) Dark current of the BNH device. Low reverse saturation current and high rectification ratio consistent with the high V_{OC} of these devices. (d) EQE spectra of the BNH device. Clear Fabry-Perot effect is observed due to large BNH thickness.

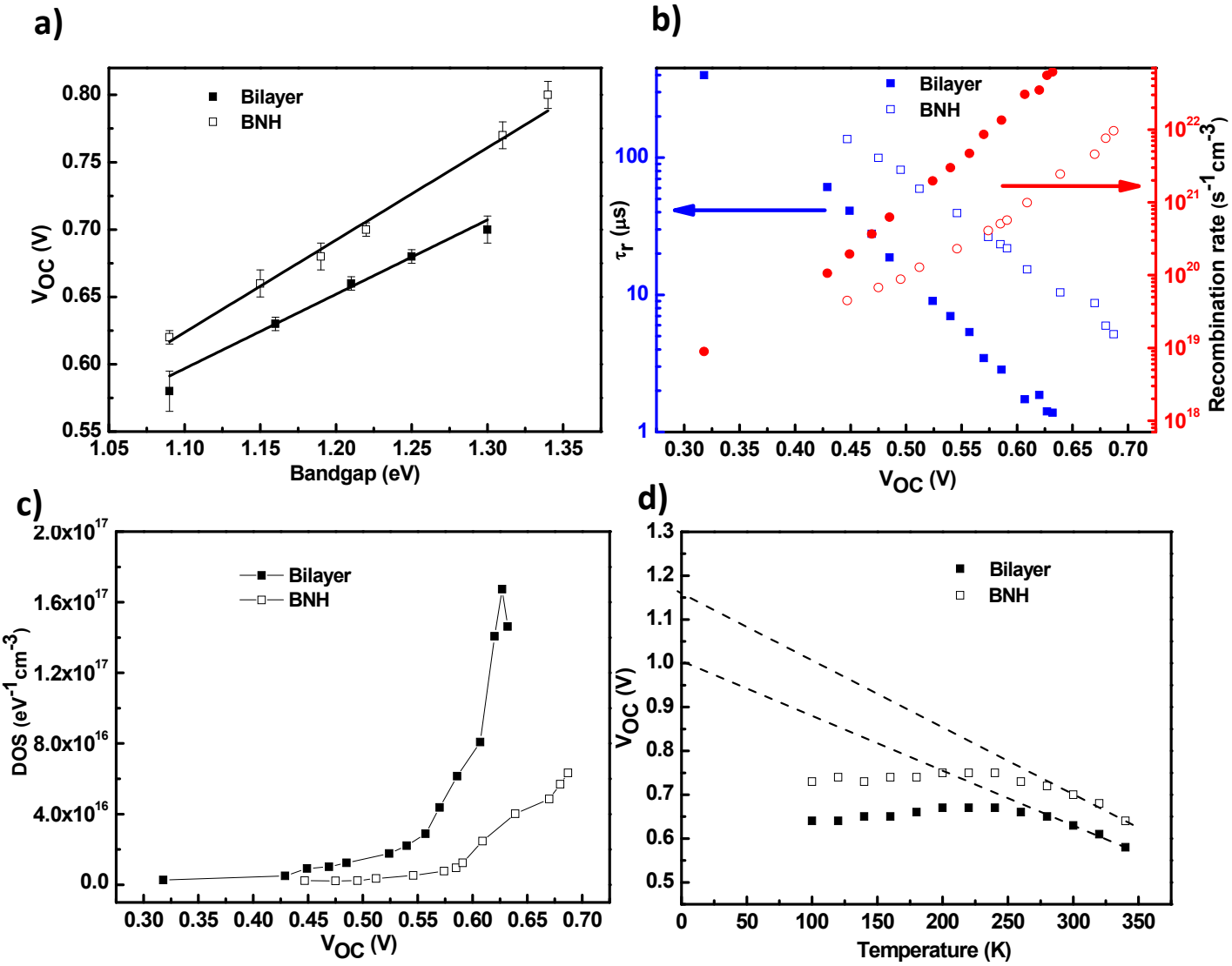

Figure 2: (a) comparison of the V_{OC} variation with PbS bandgap for bilayer and BNH device. (b) Comparison of recombination life-time (τ_r) and recombination rate of BNH and bilayer devices. The filled squares stands for bilayer devices and the open squares indicate BNH devices. (c) Density of states of the mid-gap traps obtained from TPV and TPC techniques for BNH and bilayer devices. (d) Temperature variation of V_{OC} for BNH and bilayer devices.

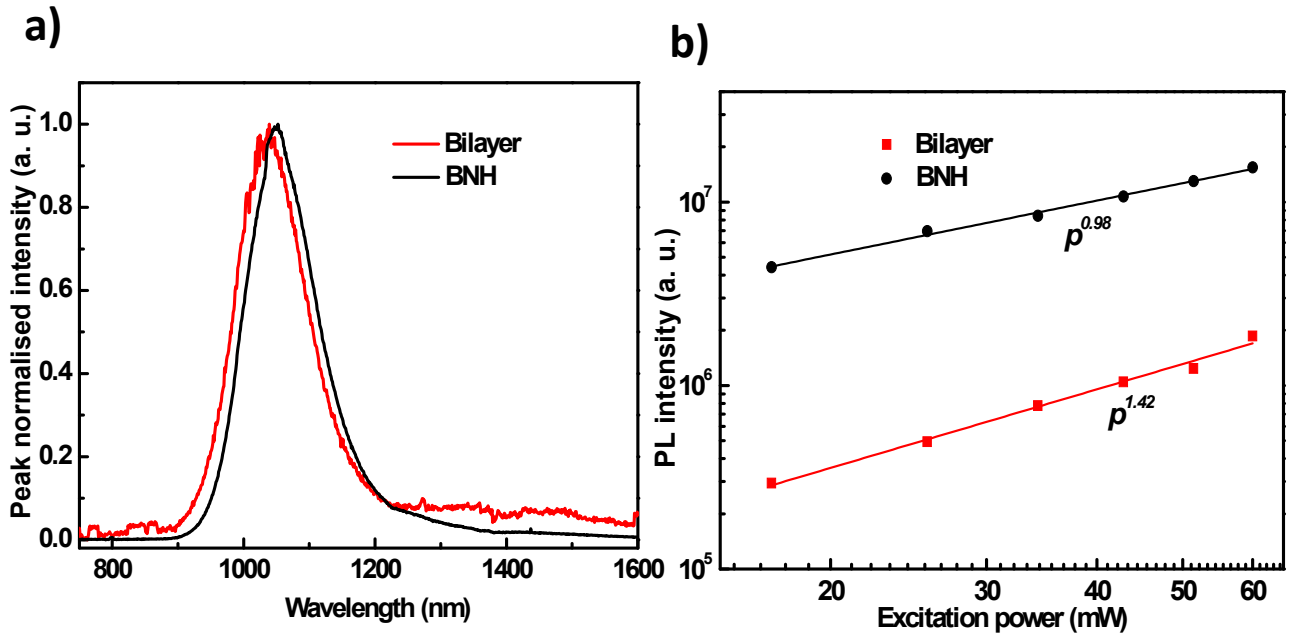

Figure 3: (a) Peak normalised PL spectra of BNH and bilayer devices. High wavelength sub-bandgap emission clearly observed for bilayer device. (b) Plot of PL intensities of band-edge emission with incident Laser power for bilayer and BNH devices.

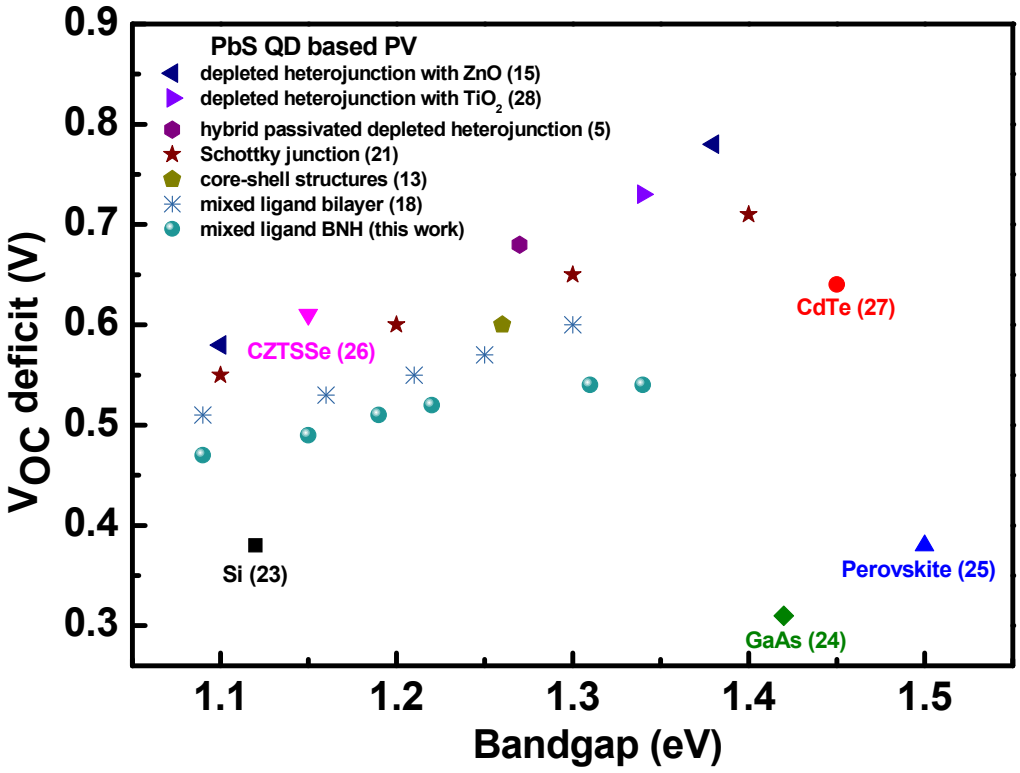

Figure 4: Calculated V_{OC} deficit for Bilayer and BNH devices and compared with other standard solar cells. Respective references are indicated in the brackets. BNH devices show the lowest V_{OC} deficit among the reported PbS QD based solar cells.

TOC:

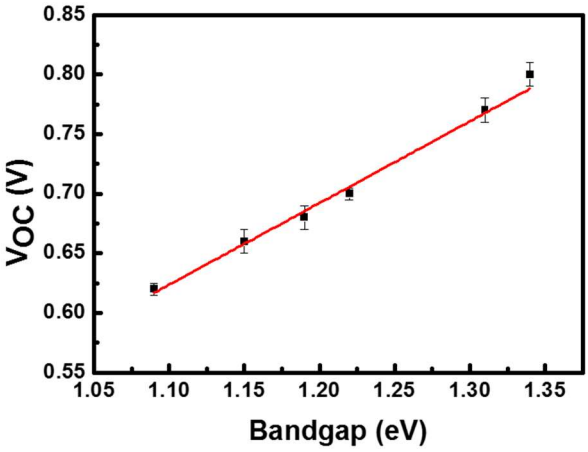
0.85
0.80
0.75
0.70
0.65
0.60
0.55
Voc (V)
1.05
1.10
1.15
1.20
1.25
1.30
1.35
Bandgap (eV)

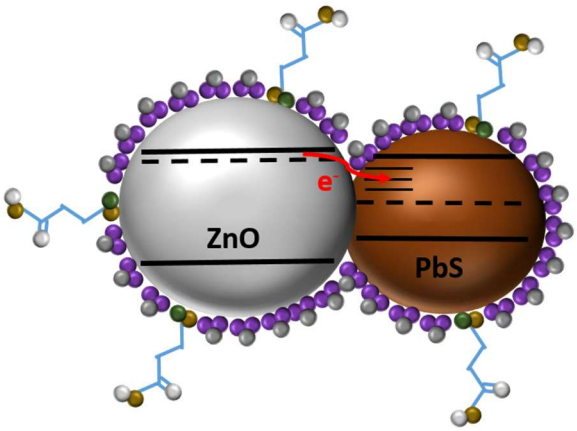
e⁻
ZnO
PbS